PART 6.
Chemistry in the Envelopes of Late-Type Stars

https://doi.org/10.1017/S0074180900164940 Published online by Cambridge University Press

Astrochemistry: From Molecular Clouds to Planetary Systems
IAU Symposium, Vol. 197, 2000
Y. C. Minh and E. F. van Dishoeck, eds.

Millimeter Observations of Molecules in the Envelopes around Late-type Stars

Michel Guélin, Robert Lucas, Roberto Neri, Michael Bremer, and Dominique Broguière

Institut de Radioastronomie Millimétrique, 300 rue de la Piscine, F-38406 St Martin d'Hères, France

Abstract. The envelopes surrounding AGB stars are similar to interstellar dark clouds in many respects; opaque to the visible light, they are transparent to mm wavelengths. Several envelopes, close enough to be spatially resolved with mm-wave interferometers, exhibit a remarkably rich molecular content, which can then be studied in detail as a function of radius. Because the envelopes are in expansion, their outer layers are older and more evolved than the inner ones, making it possible, thanks to a relatively simple geometry, to probe the time-dependence of the ongoing chemical processes.

1. Introduction

Upon reaching the end of the asymptotic Giant branch (AGB), Red Giants enter a phase of high mass loss. In less than 10^5 yr, they eject their convective envelope and the bulk of their mass. The episode of high mass loss, is capital in several respects. First of all, it contributes to the regeneration of the interstellar medium (ISM) and to its enrichment in heavy elements. Second, it disseminates the seeds of the future interstellar grains: as the gas is expelled from the hot atmosphere and expands in interstellar space, it cools off quickly, leading to the condensation of most refractory atoms and molecules; the resulting refractory grains will form the cores of the future IS dust grains. Third, the volatile compounds remaining in the gas phase expand into space where they become exposed to the interstellar UV radiation. They experience a rich photochemistry, similar in many ways to that occurring in the IS translucent clouds. The geometry and physical conditions in the expanding circumstellar envelopes (CSEs) are however much better known than in the IS clouds, making it easier to study the chemistry. In particular, it is possible in the nearest CSE to follow the changes in molecular abundance with radius, which is to say with time, and to measure the characteristic time scales for *in situ* molecule and dust formation.

After it has lost its convective envelope, the star warms up and evolves rapidly toward a Planetary Nebula. This evolution is accompanied by the rise of winds which may reach several hundreds of km s^{-1}. These superwinds and the hard UV radiation from the star, disrupt and evaporate most of the matter of the CSE leaving only a thin shiny shell, a planetary nebula (PN). The disruption of the CSE by superwinds, during the "protoplanetary nebula" phase (PPN), is

accompanied by strong shocks. The geometry is somewhat simpler than in the interstellar shocks and the time scales much shorter, which opens the prospect of observing chemical modifications in real time.

We will focus here on two envelopes: IRC+10216/CW Leo, the closest AGB star in the phase of high mass loss, and CRL 618, a nearby PPN with a spectacular molecular outflow. From considerations based on nucleosynthesis yield and isotopic composition, CW Leo is believed to be on the verge of evolving toward a PPN. Its mass loss rate ($\sim 2\,10^{-5}$ $M_\odot$ yr^{-1}) seems relatively well known, as are the physical conditions in its nearly spherically symmetrical CSE. The distance to IRC+10216 is known to be comprised between 100 pc and 300 pc. In the following, we adopt a value of 200 pc.

CRL 618, located at ~ 1.7 kpc from the Sun, consists of a thick envelope surrounding an ultra-compact HII region and a B0-type star. The central star is in a phase of high activity, judging from the presence of a fast molecular outflow. The latter, whose velocity exceeds 200 km s^{-1}, is detected in H_2 and in a number of molecules (Cernicharo et al. 1989). From high angular resolution molecular line studies, it seems that the stellar wind has just started to break through the thick CSE.

2. Photochemistry in IRC+10216

Over 50 different species, almost half of the known interstellar molecules, are observed in IRC+10216: together with the hot cores of Orion A and Sgr B2, this is the richest molecular source in the sky. This wealth of molecules is all the more remarkable in that CW Leo is a carbon star and that its outer envelope is almost devoid of oxygen-bearing molecules.

Although the ISO satellite has enlarged the number of non-polar circumstellar molecules (see Cernicharo, this volume), most of the detected species are observed through their mm or sub-mm lines. The spectrum of IRC+10216 has now been surveyed quasi continuously from the near IR to the radio cm wavelengths (Cernicharo et al. 1996; Avery et al. 1992; Groesbeck et al. 1996; Kawaguchi et al. 1995).

Figure 1 shows a portion of the $\lambda 2$ mm survey made with the IRAM 30-m telescope (Cernicharo et al. 2000). It shows cusp-shaped lines, characteristic of an expanding spherically symmetric shell. Most of the mm lines in IRC+10216 arise from refractory species and linear-carbon chain molecules not observed in the dense hot sources such as Orion A and Sgr B2. Another remarkable result is the almost complete lack of saturated C compounds and the wealth of unsaturated carbene and acetylenic chains. This abundance of metal- and Si-bearing species and of unsaturated carbon-chains, and the paucity in oxygen compounds (only CO, SiO and HCO^+ are detected) are the most remarkable features of IRC+10216's molecular composition.

The formation of such a wealth of molecular species is a challenge to the astrochemists. Most likely, it results from a three-step process: three-body reactions in the hot envelope atmosphere where the small stable compounds CO, CS, C_2H_2, HCN, SiO and SiS are formed, nucleation processes in the inner envelope which condense the refractory species at a large fraction of the carbon,

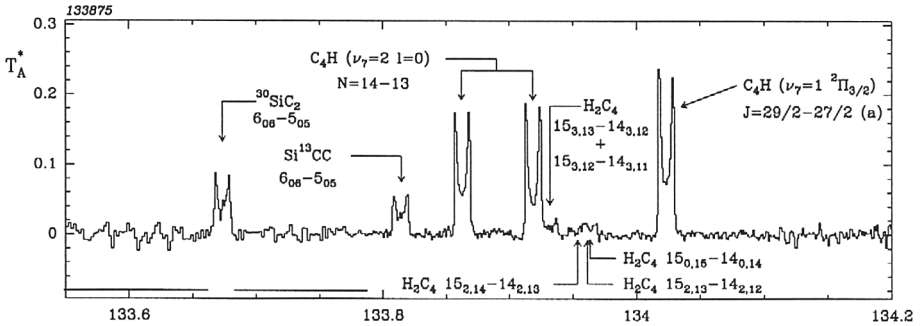

Figure 1. A portion of the 2-mm spectrum of IRC+10216 observed with the IRAM 30-m telescope (Cernicharo et al. 2000). The lines arise from refractory species or carbon-rich radicals not observed in molecular hot cores or in the terrestrial environment.

and, finally, photodissociation, ion-molecule and radical-molecule reactions in the outer envelope (see the review by Glassgold 1996).

The last step, the chemistry in the outer envelope, has been the object of particular attention. The early ion-molecule and photochemical models of Glassgold and collaborators (Glassgold et al. 1987) predicted that the parent molecules, CO, C_2H_2 and HCN, would have centrally-peaked distributions and the daughter molecules, HCO^+, CCH and CN, hollow-shell distributions. Figure 2 below and Figure 4 from Guélin et al. (1997) show that these three species are indeed confined inside a hollow shell. Statistical equilibrium calculations yield from Fig. 2 peak fractional abundances $X(HCO^+) = [HCO^+]/[H_2] \simeq 10^{-9}$, and $X(CCH) \simeq X(CN) = (1\text{–}2)\ 10^{-5}$. For all three species the peak abundance is reached at a radius $R_p = 15\text{–}18''$ ($\simeq 5\ 10^{16}$ cm).

One crucial parameter in the formation of long chain molecules in the outer CSE is time. The envelope is expanding quickly, at $v_{exp} = 14.5$ km s^{-1}, whereas the fastest two-body ion-molecule reactions proceed only with rates comparable to the Langevin rate, few $\times 10^{-9}$ s^{-1} cm^3. In view of the low abundance of the ions ($X \leq 10^{-9}$) and of the moderate gas density ($n(H_2) = 1\text{–}2\ 10^4$ cm^{-3} at the radius of interest $R = 5\ 10^{16}$ cm, or $16''$), the time scales for ion-molecule reactions (10^5 yr) are very large with respect to the time needed for the gas to flow from R=0 to R=$16''$ (10^3 yr). Cherchneff & Glassgold (1993) and Millar & Herbst (1994) have considered radical-molecule and radical-radical reactions, which, although intrinsically slower by factors ≥ 10, proceed faster as the radicals are far more abundant than the ions. The time scales for such a typical reaction:

$$C_2H + C_2H \rightarrow C_4H + H \qquad (1)$$

is a few $\times\ 10^3$ yr, not much larger than the dynamical time. Assuming C_2H is formed by the photodissociation of C_2H_2 and using networks of radical-molecule reactions similar to (1), these authors were able to reproduce the observed peak abundances of the carbon-chain molecules and radicals to better than a factor of 2 (see e.g. Guélin et al. 1998).

https://doi.org/10.1017/S0074180900164940 Published online by Cambridge University Press

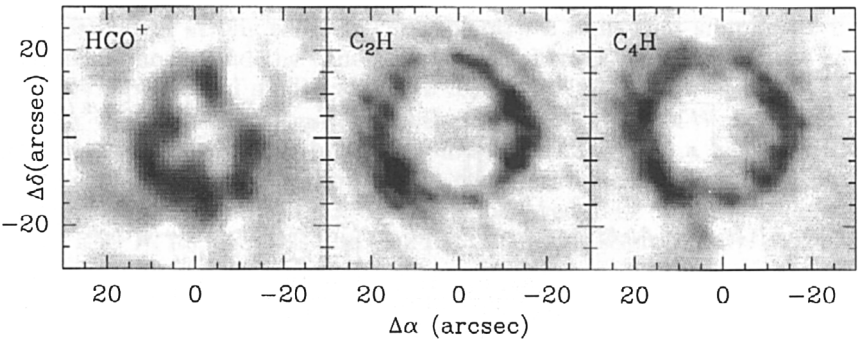

Figure 2. Brightness temperature distribution of the $\lambda 3$ mm lines of HCO^+, C_2H and C_4H, observed in IRC+10216 with the IRAM interferometer. The intensities (multiplied by 30, 1 and 2, respectively) have been integrated over a narrow band centered on the star velocity and represent roughly the species' abundance distributions in a meridian plane. The HCO^+ map has a factor of two poorer resolution and a 30 times weaker intensity than the C_2H map; it is therefore much noisier. It shows nevertheless clearly a hollow-shell type distribution. Note that the C_2H map, which has the highest signal-to-noise ratio, shows a double-shell structure to the NW; such a structure is also visible in the high S/N ratio maps of CN and HNC (see Fig. 4 of Guélin et al. 1997).

The agreement between the observed and predicted peak abundances does not mean, however, that the formation of the long carbon chains is understood. In the above models, the key bricks for long carbon chain formation are C_2H_2 and its photodissociation product C_2H. The longer chains form from shorter ones and, thus, appear later and at larger radii. C_4H, for example, reaches an abundance of $X=10^{-6}$, at which C_4H and C_2H are both easily detectable, at a radius $R=4\ 10^{16}$ cm, 1.6 times larger than C_2H, and C_6H the same abundance at a radius $R=7\ 10^{16}$ cm, 1.6 times larger than C_4H and 2.6 times larger than C_2H (Millar & Herbst 1999, priv. comm.). A similar shift is predicted between HC_3N and HC_5N (Glassgold 1996).

These shifts are not observed. The distributions of C_2H, C_4H and C_6H are remarkably similar and all three species start to be observed –and reach an abundance of 10^{-6}– at the same radius (see e.g. Fig. 2). The same also applies for HC_3N and HC_5N (Figure 3): there is a remarkable coincidence between the brightness distributions of HC_5N and $HC^{13}CCN$ (we use this rare isopomer rather than the abundant one, as its line intensity is comparable to that of HC_5N). Both distributions coincide to better than $2''$, so that both species must have formed quasi-simultaneously (i.e. within 150 yr).

The remarkable correlation between the brightness distributions of HC_3N and HC_5N and, more generally, between all carbon chain molecules and radicals would be easy to understand if these distributions reflected the total gas distribution and/or the excitation conditions, rather than a change in chemical composition. This does not seem to be the case. Figure 4 shows the brightness

https://doi.org/10.1017/S0074180900164940 Published online by Cambridge University Press

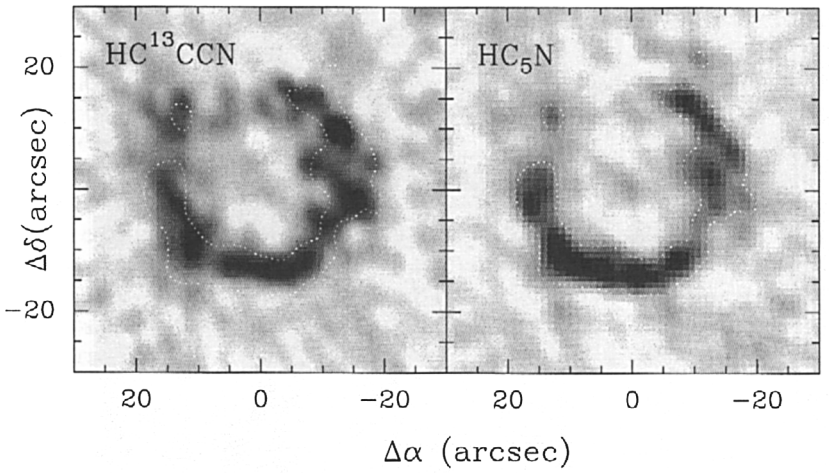

Figure 3. Brightness temperature distribution of the λ 3 mm lines of $HC^{13}CCN$ and HC_5N, observed in IRC+10216 with the IRAM interferometer. The $HC^{13}CCN$ line intensity has been multiplied by 2 to match the HC_5N one. The dotted white line marks the outer contours of the HC_5N emission: note the great similarity between the two maps.

distributions of the J=1–0 line of ^{13}CO, observed with the IRAM interferometer: in contrast to the broad and smooth, centrally peaked ^{13}CO brightness distribution observed with the 30-m telescope, the interferometer maps (which filter out the structures larger than 20″) reduce to a central peak. They show no conspicuous clumpy ring-like structure which would mimic the rings visible in Figure 3.

We have modelled with a 3-D Monte-Carlo radiative transfer code (Gonzalez 1995; Gonzalez et al. 2000) the ^{13}CO brightness distribution seen by the interferometer in the case of an expanding spherical envelope with a density distribution $n(H_2) \sim R^{-2}$, corresponding to a mass loss rate of 2 10^{-5} $M_\odot$ yr^{-1}, a fractional CO abundance of 8 10^{-4}, and a $^{12}CO/^{13}CO$ abundance ratio of 40; the gas kinetic temperature was taken as a power-law with 60 K at 12″ radius and 1028 K at 5 R_*.

Figure 4b (v=−26 km s^{-1}), shows how easily one would see isobaric clumps. Four such condensations have been introduced in 90° spacings around the central source: two (offset 11″S and 11″W) have a diameter of 7″ and the two other (offset 8″N and 8″E) a diameter of 3″. The density contrast of the clumps relative to the underlying spherically-symmetric gas distribution is 2 in the cases of the E and W clumps and 4 for the N and S clumps. The clump 11″S of the source appears brighter than any feature, except for the central source, in the observed v=−26 km s^{-1} map. Note that in the simulation (b) as in the observed map (a), the spherically-symmetric envelope is detected only near its central peak and appears much stronger at the terminal velocity than at the star systemic velocity.

https://doi.org/10.1017/S0074180900164940 Published online by Cambridge University Press

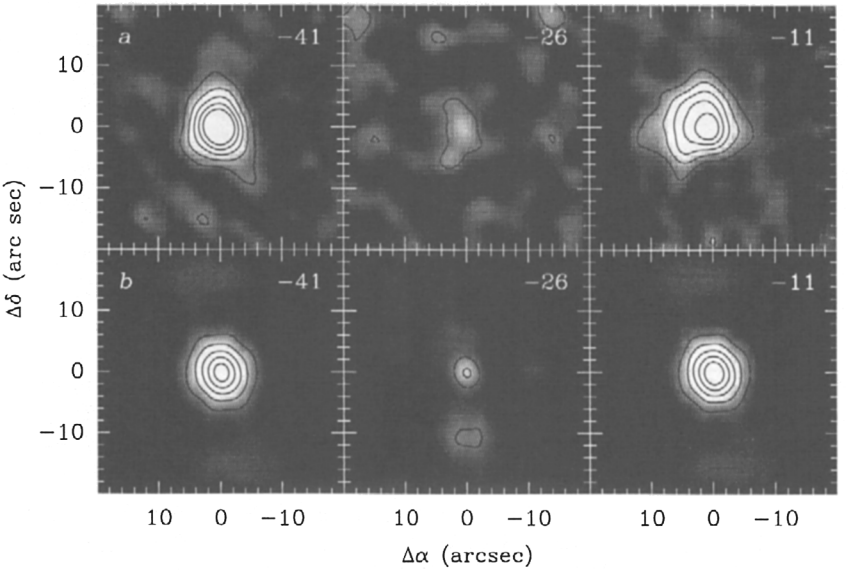

Figure 4. Velocity-channel maps showing the emission in the J=1–0 line of ^{13}CO, observed with the IRAM Plateau de Bure Interferometer (a) *(upper 3 maps)*. The *bottom 3 maps* of the figure (b) show the brightness distributions which would be observed with the interferometer in the case of clumps superimposed on a spherically symmetric distribution with a density $n(H_2) \sim R^{-2}$ (see text). The channel velocity is indicated in the upper left corner of each map; the channel width is 1 km s^{-1}. The central images correspond to the star systemic velocity ($v_{sys} = -26$ km s^{-1}) and the left and right images to the envelope terminal velocity ($v_{sys} \pm v_{exp}$). The envelope emission is almost fully resolved in the central interferometer map.

From the comparison of the simulated and observed ^{13}CO maps, we conclude that the column density enhancement in the 16″ ring does not exceed a factor of 3, and that the volume density in the clumps is unlikely to exceed 5 10^4 cm^{-3}.

Another interesting piece of information comes from the deep CFHT optical images reported by Mauron & Huggins (1999). These images show the ambient Galactic light scattered by the dust in the outer envelope. They reveal a succession of incomplete shells, the innermost of which follow in the NW the two shells visible in the C_2H, CN, and HNC maps. The density contrast which can be inferred between the shells and the inter-shell regions reaches factors of several at large radii ($R > 30''$), but hardly exceeds, even locally, a factor of 3 for the shells with R=15–20″, the observed surface brightness contrast between the rim and the dips being everywhere ≤ 1.5.

Finally, the overall similarity between the intensity distributions of the C_2H line, which is easily collisionally excited because of the low dipole moment, and

https://doi.org/10.1017/S0074180900164940 Published online by Cambridge University Press

of the $HC^{13}CCN$ line, which is hard to excite, argue also against a high volume density enhancement.

The factor of 3 limit on the density enhancement means, first, that the ring structure in Figure 3 reflects mainly a change in the chemical composition and, second, that the average density in the clumps is probably not high enough to reduce the formation time of C_4H through reaction (1) to ≤ 150 yr. New computations would be needed, however, to demonstrate this point.

In conclusion, the long cyanopolyynes and C-chain radicals must form quasi-simultaneously in the outer CSE. Their formation times seem incompatible with the molecule-radical reaction models proposed so far, which assume a constant mass loss rate. Models with mass loss rate varying by factors of 2–3 should be investigated. Different, faster processes, such as the release of radicals from the grains caused by the impinging of interstellar photons or by mild shocks, might have to be invoked (Guélin et al. 1993).

3. Shock Chemistry in CRL 618

Stars evolving off the AGB to become planetary nebulae undergo a short-lived phase of spectacular mass-loss: they develop high velocity outflows of gas and dust which appear as two symmetric lobes arising from the obscured star. CRL 618 is nowadays the best known example of a carbon star in such a high activity stage. The elongated ultra-compact HII region of size $< 1''$, which surrounds the star, has increased tenfold its cm flux in the 80's. Its 3-mm flux, measured with the Bure interferometer, has increased by another 50% in the last decade.

Over 10 molecular species were observed in CRL 618 at millimeter wavelength, several of which are detected in both the dense CSE and the high velocity outflow: CO, CN, HCN, HC_3N. The 3-mm lines of HCN, ^{13}CO and ^{12}CO, have been mapped with the IRAM, OVRO, and Nobeyama interferometers (Neri et al. 1992; Yamamura et al. 1994; Hajian et al. 1996).

New results of IRAM interferometric observations in the lines of ^{12}CO (J=2–1) and HC_3N (J=25–24) are presented in Figure 5. They show the high degree of symmetry of the nebula as traced by these molecules. Both position-velocity cuts show a complex spatio-kinematical pattern with two outstanding substructures: a large CSE with a centrally-peaked distribution, remnant of the AGB phase, and a strong bipolar emission with projected velocities up to ~ 200 km s^{-1}. Blue-shifted emission is observed to the East, red-shifted emission to the West. Blue-shifted absorption features give further evidence for high velocity gas flowing outwards from the immediate vicinity of the central star. CO being easier to excite than HC_3N is well-detected further out.

These observations were made with a $\sim 1''$ resolution, but the high signal-to-noise ratio of the data, which allow the positioning of the emission wings to better than a tenth of an arcsec, confirms the remarkable result already reported by Neri et al. (1992): the existence of post-shock regions where high-velocity molecular gas is reformed in the envelope surrounding CRL 618. Most likely, the wings of the CO and HC_3N lines and of other molecules arise from these regions. The small size and the positions of the regions corroborate the idea that the star has reached a stage where the high velocity winds are just

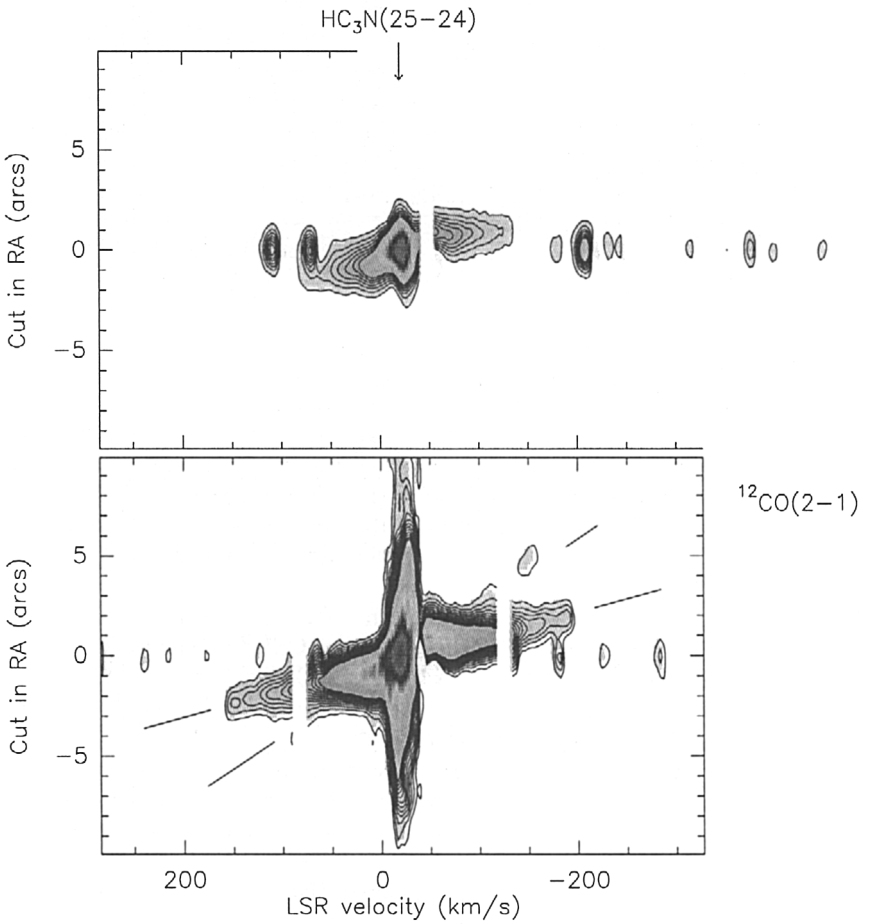

Figure 5. Position-velocity diagrams along the E-W axis of CRL 618 for the emissions in the ^{12}CO (J=2–1) and HC_3N (J=25–24) line, observed with a 2″ resolution with the IRAM interferometer. The emission hole at $-70 \leq v \leq -35$ km s^{-1} results from the absorption of the compact HII region by the foreground outflowing gas.

https://doi.org/10.1017/S0074180900164940 Published online by Cambridge University Press

scraping through the dusty envelope, inducing shocks in the surrounding nebular material. We are tempted to identify the emission wings with post-shock formed molecular gas streaming down from these regions. In view of the short time scale at which the compact HII region and the star seem to evolve, CRL 618 might be one of the very few objects where chemical composition changes could directly be observed within few years.

Acknowledgments. We are grateful to Nicolas Mauron and Patrick Huggins for communicating us their scattered radiation maps prior to publication and E. Herbst and T. Millar for showing us the results of their abundance calculations. E. Gonzalez, R. Gruenewald and J. Cernicharo participated in the conception and writing up of the 3-D radiative transfer code.

References

Avery, L., Amano, T., Bell, M.B., et al. 1982, ApJS, 83, 367
Cernicharo, J., et al. 1989, A&A, 222, L1
Cernicharo, J., Barlow, M.J., Gonzalez-Alfonso, E., et al. 1996, A&A, 315, L201
Cernicharo, J., Guélin, M., & Kahane, C. 2000, A&A, in press
Cherchneff, I. & Glassgold, A.E. 1993, ApJ, 419, L41
Glassgold, A.E., Mamon, G.A., Omont, A., & Lucas, R. 1987, A&A, 180, 183
Glassgold, A.E. 1996, ARAA, 34, 241
Gonzalez, E. 1995, PhD thesis, Madrid
Gonzalez, E., Broguiere, D., Bremer, M., et al. 2000, in preparation
Groesbeck, T.D., Phillips, T.G., & Blake, G.A. 1994, ApJ, 428, 680
Guélin, M., Lucas, R., & Cernicharo, J. 1993, A&A, 280, L19
Guélin, M., Lucas, R., & Neri, R. 1997, in CO: Twenty-Five Years of Millimeter Radio Astronomy, eds. W.B. Latter et al., 359
Guélin, M., Neininger, N., & Cernicharo, J. 1998, A&A, 335, L1
Hajian, A.R., Phillips, J.A., & Terzian, Y. 1996, ApJ, 467, 341
Kawaguchi, K., Kasai, Y., Ishikawa, S., & Kaifu, N. 1995, P.A.S.J., 47, 853
Mauron, N. & Huggins, P.J. 1999, A&A, 349, 203
Millar, T.J. & Herbst, E. 1994, A&A, 288, 561
Neri, R., et al. 1992, A&A, 262, 544
Yamamura, I., Shibata, K.M., Kasuga, T., & Deguchi, S. 1994, ApJ, 427, 406

Discussion

A. Lapinov: Is it possible to locate the HCN maser position in IRC+10216?

M. Guélin: It coincides with the star position.

E. F. van Dishoeck: Can you comment briefly on your observations of sources other than IRC+10216? Do they show the same coincidence of carbon-chain species?

M. Guélin: IRC+10216 is by far the closest AGB star envelope with a thick envelope. CIT6, which is a factor of ~ 5 farther, seems to show the same gross spatial distribution features, but the signal weakness and lower achievable spatial resolutions do not allow a detailed comparison of the peak abundance values for the time being. ALMA will allow such studies in the future. As concerns planetary nebulae, their envelopes are detected from the star and the coincidence between the different molecular species only reflects the confinement of the gas in the narrow shells.

https://doi.org/10.1017/S0074180900164940 Published online by Cambridge University Press